Nickel-Based Catalyst Supported on Porous Carbon Carrier with Hydrophilic Domains Enables High-Performance Anion Exchange Membrane Fuel Cells

Pin Meng, Peichen Wang, Jiahe Yang, Yunlong Zhang, Hongda Shi, Xingyan Chen, Dingge Fan, Siyan Chen, Xi Lin, Dongdong Wang, Yang Yang, Qianwang Chen**

Hefei National Research Center for Physical Sciences at the Microscale and Department of Materials Science and Engineering, University of Science and Technology of China, Hefei 230026, China

Corresponding Author's E-mail: yangyang1991@ustc.edu.cn (Y. Yang), cqw@ustc.edu.cn (Q. Chen).

Experimental Section

Methods Materials. Zinc acetate dihydrate (99.0%, SCR), 2-Aminoterephthalic acid (> 98.0%, Aladdin), Nickel acetylacetonate (99.0%, SCR), Ethanol (≥ 99.5%, SCR), Methanol (≥ 99.5%, SCR), Triethylamine (≥ 99.0%, SCR), N, N-Dimethylformamide (≥ 99.5%, SCR), Potassium hydroxide (≥ 85.0%, SCR), Oleylamine (≥ 70.0%, Sigma), Oleic acid (99.0%, SCR), Triethylamine borane (97.0%, Aladdin), Nafion solution (~5% in a mixture of lower aliphatic alcohols and water, DuPont), commercial 20wt.% Pt/C catalyst were purchased from Hesen and commercial 40 wt.% Pt/C was purchased from johnson matthey.

Synthesis of IRMOF-3

IRMOF-3 was prepared by a modification of a reported method[1]. In brief, 7 g Zn $(CH_3COO)_2 \cdot 2H_2O$ was dissolved in 80 mL DMF at room temperature, and 2 g 2-aminoterephthalic acid was directly poured into the former solution. After the solid powder was completely dissolved, the solution was stirred at room temperature for 15 minutes, and 4 mL triethylamine was added by injection. The resulting solution was then stirred at 125℃ for 24 h. The obtained sample was repeatedly cleaned with DMF and methanol, and finally placed in a vacuum drying oven at 60℃ for use.

Synthesis of Zn_1-NC

200 mg IRMOF-3 was soaked in 80mL methanol for three days to purify IRMOF-3 for reserve use. The obtained solid powder was centrifuged, washed and dried for use. Subsequently, the precursor was annealed in a tube furnace, and the specific experimental details were as follows: the temperature was held for 2 h at 650℃, the heating rate was 5℃ min^{-1}, and the H_2/Ar ratio was 1.5/73 (mL min^{-1}). The obtained black powder was placed in 3 M hydrochloric acid for etching to remove the surface zinc oxide. After washing and drying, the required sample was finally obtained, and the sample was named Zn_1-NC.

Synthesis of Ni/Zn_1-NC and Ni/rGO.

The Ni/Zn_1-NC was synthesized by modifying a previous method[2]. 50 mg of Zn_1-NC powder was dispersed in 25 mL of oleylamine and 0.5 mL of oleic acid under sonication for 30 min. Afterwards, 2 mmol $Ni(acac)_2$ was added to the above solution under magnetic stirring. The solution was continuously heated to 110℃ under vacuum to remove O_2 and H_2O and naturally cooled to 90℃ under an Ar atmosphere. Then 0.64 mL of triethylamine borane was injected into the solution under stirring for 1 h. Finally, the sample was thoroughly washed with ethanol and dried in an oven at 60℃ for 12 h to obtain black precursor. The precursor was annealed inside a tube furnace at 400℃ for 2 h under 7.5% H_2/Ar atmosphere to form Ni/Zn_1-NC. For comparison, the sample prepared with rGO instead of Zn_1-NC as the support was named Ni/rGO.

Materials characterization.

The powder X-ray diffraction (XRD) patterns of the samples were collected from a Japan Rigaku D/MAX-γA X-ray diffractometer equipped with Cu Kα radiation (λ=1.54178 Å). Transmission electron microscopy (TEM) images were recorded with

a Hitachi H-7650 transmission electron microscope using an accelerating voltage of 200 kV, and high resolution transmission electron microscope (HRTEM) (JEOL-2011) was operated at an acceleration voltage of 200 kV. X-ray photoelectron spectroscopy (XPS) was carried out using a Thermo ESCALAB 250Xi photoelectron spectrometer instrument. XAFS analyses were performed with Si (111) crystal monochromators at the BL14W1 beam Line at the Shanghai Synchrotron Radiation Facility (SSRF, Shanghai, China). The XAFS spectra were recorded at room temperature using a 4-channel Silicon Drift Detector (SDD) Bruker 5040. The extended X-ray absorption fine structure (EXAFS) spectra were recorded in transmission/fluorescence mode. Thermogravimetric analysis (TGA) measurements were carried out on NETZSCH TG 209 F1 Libra. Samples were heated from 30 to 800 °C at a ramp rate of 10 °C min^{-1}. The ultraviolet photoelectron spectroscopy (UPS) and work function of the material were tested at the Surface and catalytic line station of the National Synchrotron Radiation Laboratory, USTC. This beamline is connected to an undulator and equipped with two gratings that offer soft X-rays from 20 to 600 eV with a typical photon flux of 5×10^{10} photons/s and a resolution($E/\Delta E$) better than 10^5 at 29 eV. This system is comprised of four ultrahigh vacuum (UHV)chambers including analysis chamber, preparation chamber, molecular beam epitaxy (MBE) chamber, and a radial distribution chamber. The base pressures are7×10^{-11}, 1×10^{-10}, $5\times10^{-10}$and 2×10^{-11} mbar, respectively. A sample load-lock system is connected to the sample transfer chamber. The analysis chamber is equipped with a VG Scienta R4000 analyzer, a monochromatic Al *Ka* X-ray source, a UV light source, low energy electron diffraction (LEED), a flood electron gun, and a manipulator with high precision and five-degree-of-freedom. The preparation chamber comprises an ion gun, a quartz crystal microbalance (QCM), a residual gas analyzer, a manipulator with high precision and four-degree-of-freedom, and several evaporators. The MBE chamber houses a QCM, several evaporators and a manipulator with two-degree-of-freedom. With this radial distribution chamber, the time for each transfer process between two chambers is less than 1 minute. An inductively coupled plasma optical emission spectrometer (ICP-OES) was utilized to determine the metal loading of the samples using an Optima 7300 DV instrument.

Electrocatalytic measurements details.

All electrochemical tests were carried out at the CHI 760E electrochemistry workstation. The GCE loaded with electrocatalysts served as the working electrode, the platinum wire served as the counter electrode and the Ag/AgCl electrode served as the reference electrode. In this work, all the measured potentials were referred to the reversible hydrogen electrode (RHE) potential. For HOR electrochemical test, 0.1 M KOH was used as the electrolyte. Before HOR tests, the catalyst ink was cast onto a 5-mm-diameter glassy carbon RDE to form a thin film layer, Then, cyclic voltammetry (CV) was conducted in H_2-saturated electrolyte to obtain the steady voltammetry curves, and the polarization curves were recorded using a rotating disk electrode (RDE) with a rotation speed of 1,600 rpm in H_2-saturated electrolyte for HOR. Electrochemical impedance spectra (EIS) tests were carried out after each RDE

measurement. The real part of the resistance was used to obtain the iR-free potential for all the potential data of HOR in this work. The catalyst ink was prepared by dispersing 4 mg of catalyst in a mixed solution consisting 480 μL of ethanol and 20 μL of Nafion solution (Du Pont, 5 wt.%). The above suspension was sonicated in an ice bath to form catalyst ink. Then, 15 μL of the catalyst ink was dropped onto the polished glassy carbon electrode with a total catalyst loading (including metal and carbon support) of 0.612 mg cm^{-2}.

To calculate the kinetic current density, the Koutecky–Levich equation (equation (1)) was used to describe a process controlled by both kinetics and diffusion:

$$\frac{1}{j} = \frac{1}{j_k} + \frac{1}{j_d} = \frac{1}{j_k} + \frac{1}{Bc_0\omega^{1/2}} \quad (1)$$

where j_k is the kinetic current density and j_d is the diffusion-limited current density, B is the Levich constant, c_0 is the solubility of H_2 in the electrolyte, and ω is the rotating speed. j_d can be further expanded according to the Levich equation (equation (2)):

$$j_d = nFD^{2/3}\nu^{-1/6}c_0\omega^{1/2} = Bc_0\omega^{1/2} \quad (2)$$

where n is the electron transfer number during the reaction, F is Faraday's constant, D is the diffusion coefficient of H_2 and ν is the kinematic viscosity of 0.1M KOH. The exchange current density j_0 can be obtained by fitting j_k and η to the Butler–Volmer equation (equation (3)):

$$j_k = j_0\left(e^{\frac{\alpha F}{RT}\eta} - e^{\frac{-(1-\alpha)F}{RT}\eta}\right) \quad (3)$$

where α is charge transfer coefficient, F is Faraday's constant (96,485 C mol^{-1}), R is the universal gas constant (8.314 J mol^{-1} K^{-1}), T is the room temperature and η is the overpotential. The obtained Tafel plot is shown in Figure 2b. Extrapolating the curve with fitted j_0 and α, j_k was calculated at η=50 mV using this method.

Due to the scarcity of samples under the test conditions of RDE, it is difficult to conduct characterization after accelerated durability tests (ADT) testing. Therefore, the characterization tests after ADT testing are all obtained after gas diffusion electrode (GDE) testing.

***In-situ* ATR-SEIRAS experiments**

The attenuated total reflectance surface-enhanced infrared absorption spectroscopy (ATR-SEIRAS) experiments were taken with Nicolet iS50 FT-IR spectrometer equipped with an MCT detector cooled with liquid nitrogen and PIKE VeeMAX III variable angle ATR sampling accessory 64 interferograms were co-added for each spectrum. The spectra were given in absorption units defined as$A = -\log(R/R0)$, where R and R0 represented the reflected IR intensities corresponding to the sample and reference-single beam spectrum, respectively. A 60° Si face-angled crystal was used as reflection element. The angle of incidence was set as ca. 70°. The ultra-thin Au film was deposited chemically in it for IR-signal enhancement and conduction of electrons. The electrocatalyst was dropped onto Au film to serve as a working electrode for SEIRAS experiments. A platinum wire and an SCE electrode were used as counter and reference electrode in all tests, respectively. The H_2-saturated 0.1 M KOH was used as the electrolyte. Chronopotentiometry method was used in this experiment at different potentials (0 to 0.2 V versus RHE without iR-correction). The

SEIRAS spectra were collected during the chronopotentiometry test.

The experiments of potential of zero charge (PZC)

The E_{PZC} of the catalysts were measured via capacitance from EIS data in 5 mM Ar-saturated NaF soltuon with a carbon rod and Ag/AgCl (saturated KCl) as counter and reference electrode, respectively. The electrochemical impedance spectroscopy (EIS) measurements for E_{PZC} were conducted at a frequency of 1 Hz with a potential increment of 10 mV. The value of E_{PZC} was decided from the minimum of specific capacitance. We conducted EIS and calculated the minimum value of the specific capacitance (C) versus the potential to obtain the PZC of the catalysts. The C was determined from the imaginary part, Z_{im}, of the impedance using the following equation (equation (4)).

$$C = -(\omega Z_{im})^{-1} \quad (4)$$

AEMFC assembly and testing

The electrode ink was prepared by adding the catalyst, additional Vulcan XC-72 carbon for anode ink only and ionomer to isopropanol and H_2O as solvent, followed by sonication for 1 h. The weight ratio of the Vulcan XC-72 and Ni/Zn_1-NC catalyst was 1:2, and the weight ratio of the PAP-TP-100 ionomer and carbon support was approximately 0.33 for both the anode and cathode. Next, the anode ink was sprayed onto one side of the membrane (PAP-TP-85, Versogen) with a loading of 1.33 mg_{Ni} cm^{-2} and the cathode ink was sprayed onto the other side of the membrane with a loading of 0.22 mg_{Pt} cm^{-2} for Pt/C. After drying at room temperature, the Membrane electrode assembly (MEA) was immersed in 3M KOH aqueous solution for 2 h to remove CO_2 absorbed by the catalyst layers. The residual KOH solution on the MEA would then be rinsed before testing. The MEA was assembled with a fluorinated ethylene propylene gasket, a piece of carbon paper (Sigracet SGL 28 BC) as the gas diffusion layer on the cathode side, a graphite bipolar plate with 5 cm^{-2} flow field and a gold-coated current collector on each side to complete the full AEMFC. A fuel cell test station (Scribner 850e) with back-pressure regulators was used to measure the polarization curves and stability under H_2/O_2 or H_2/CO_2-free air conditions. The overall PGM loading was analyzed using ICP-AES. It should be emphasized that the contact time between the synthetic catalyst and the air should be minimized as much as possible, and the testing speed of the AEMFC components should be accelerated.

After the cell equilibrated at the desired conditions for around 30 min, polarization curves were obtained by scanning from OCV (~1 V) to approximately 0.2 V with voltage steps of 50 mV and held at each point for 5 s[3].

In constant current mode, the impedance spectrum between 20 kHz and 0.1 Hz is recorded at various current densities, with the amplitude set to 10% of the DC current. To obtain distribution of relaxation times (DRT), we followed the approach of Saccoccio et al.[4] and Wan et al.[5] as described in their publications and their open-source software, DRT tools.

DFT calculations

The density functional theory (DFT) calculations were performed using the Vienna Ab Initio Simulation Package (VASP)[6][7], and the generalized gradient approximation (GGA)[8] of Perdew-Becke-Ernzerhof (PBE)[9] was used for the exchange-correlation

functional. The cut-off energy was set to 400 eV for the plane-wave expansion of the electronic wave function. All structures were optimized with a convergence criterion of 1×10^{-5} eV for the energy and 1×10^{-7} eV for the frequency. The rGO and Zn_1-NC models to calculate were built in slab model with the size of 14.76*14.76 Å, and the height of the vacuum layer was greater than 15 Å to avoid interlayer interaction. The lattice of original Ni was optimized and reconstructed as Ni (100) surface with its edge lengths fit the size of the cell box of optimized rGO and Zn_1-NC to form Ni/rGO and Ni/Zn_1-NC structure. For subsequent static calculations and Bard charge calculations, the Monkhorst-Pack k-point sampling is set to 3*3*1. The charge difference was computed through the following equation: $\rho_{diff} = \rho_{Ni/rGO} - \rho_{rGO} - \rho_{Ni}$ and $\rho_{diff} = \rho_{Ni/Zn1\text{-}NC} - \rho_{Zn1\text{-}NC} - \rho_{Ni}$. The binding energy were calculated as follow: $E_{be} = E_{Ni/Zn1\text{-}NC} - E_{Zn1\text{-}NC} - E_{Ni}$ and $E_{be} = E_{Ni/rGO} - E_{rGO} - E_{Ni}$.

Supplementary Notes

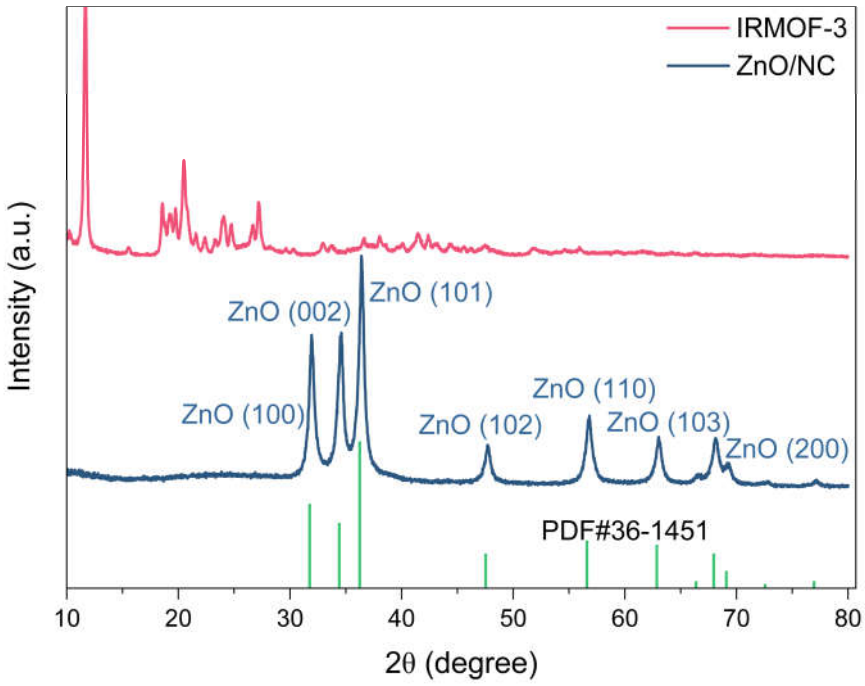

Figure S1. XRD pattern of IRMOF-3 and ZnO/NC.

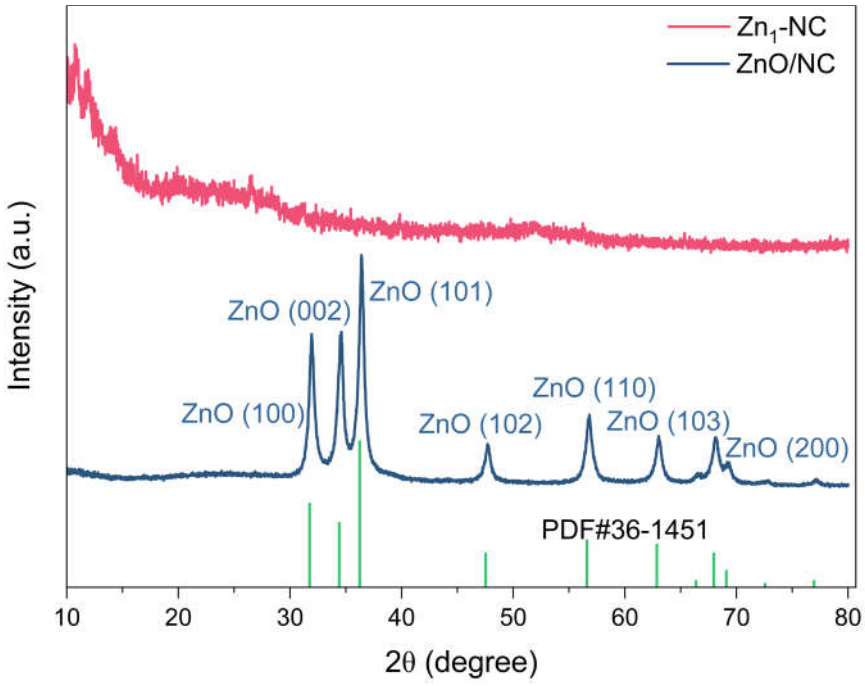

Figure S2. XRD pattern of Zn_1-NC and ZnO/NC.

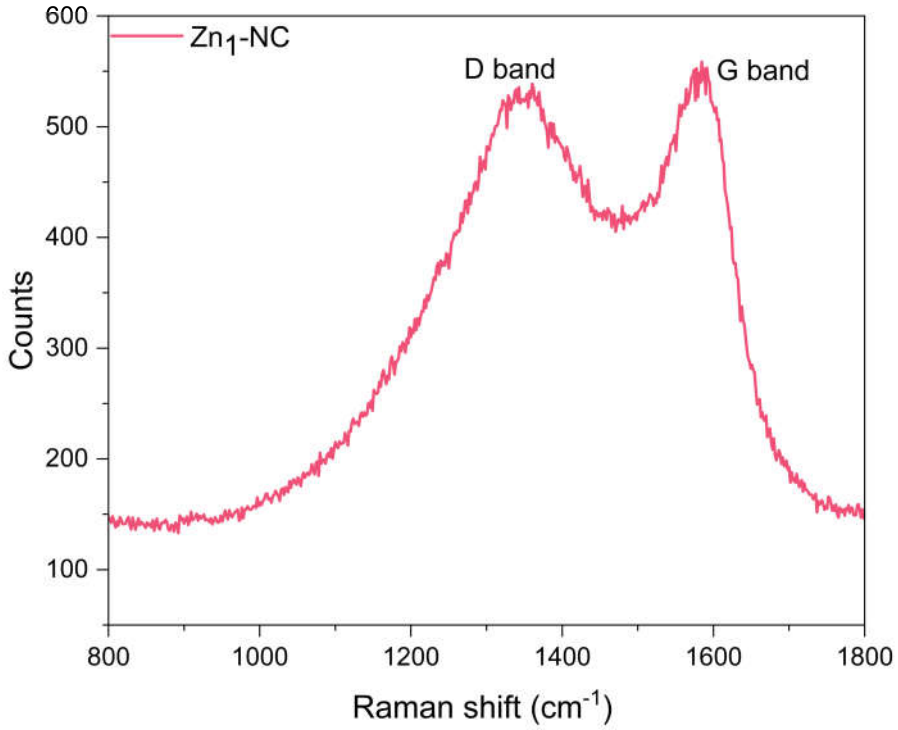

Figure S3. Raman spectrum of Zn_1-NC.

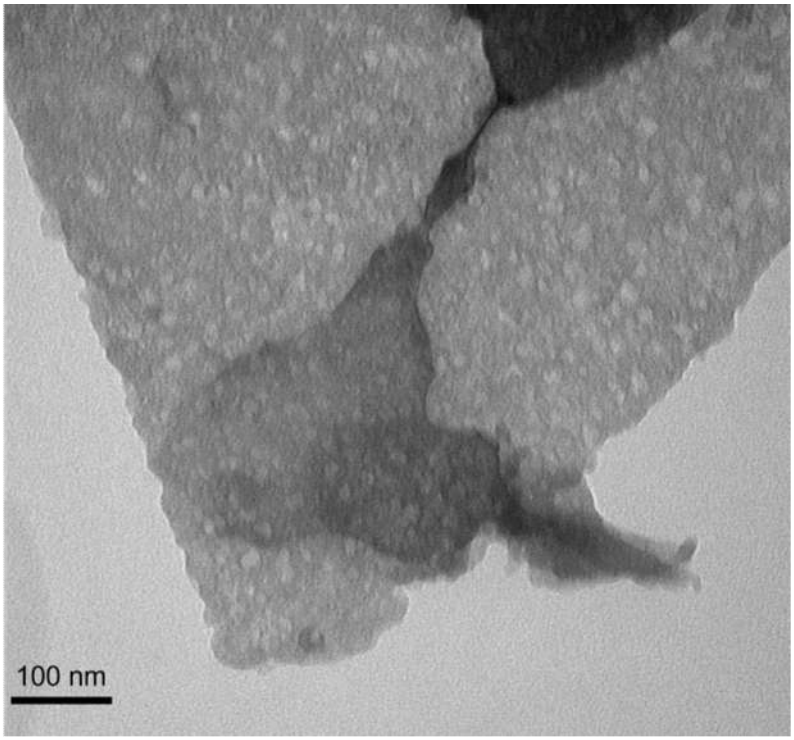

Figure S4. TEM images of Zn_1-NC.

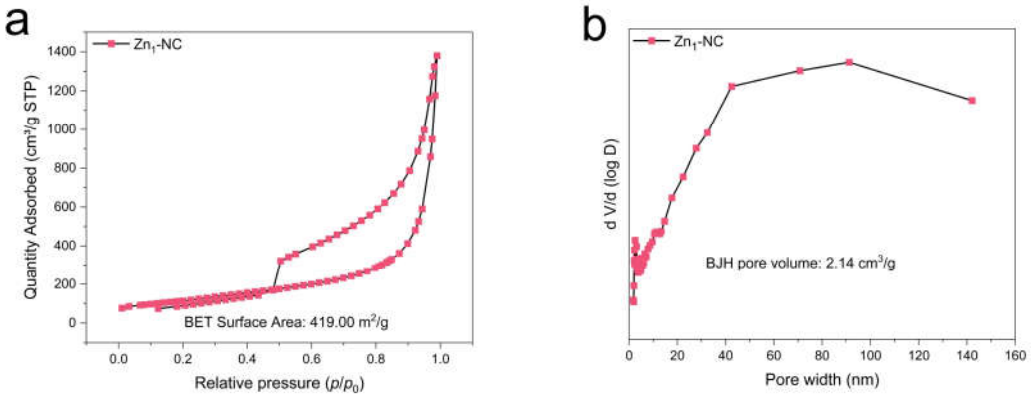

Figure S5. (a) N_2 adsorption-desorption isotherm and (b) pore distribution analysis for Zn_1-NC.

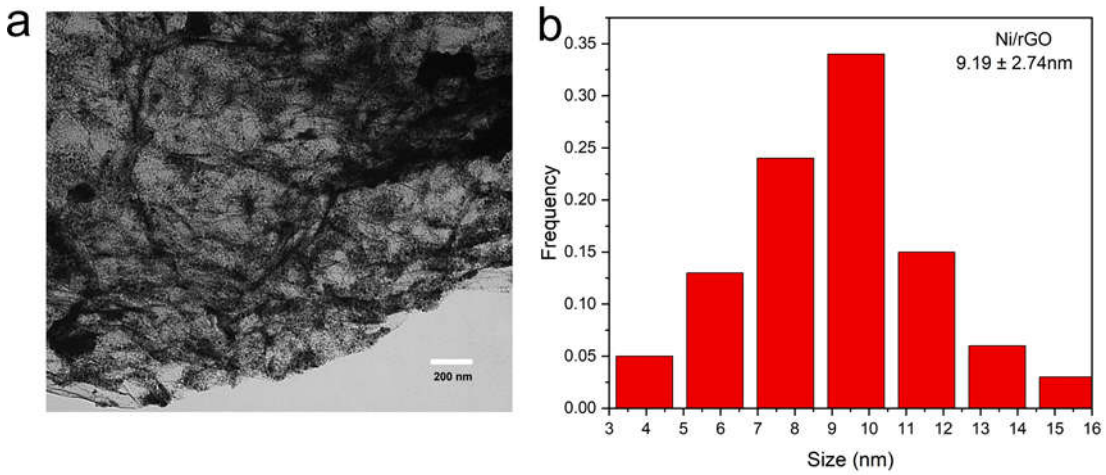

Figure S6. (a) TEM image of Ni/rGO and (b) the size distribution of nanoparticles.

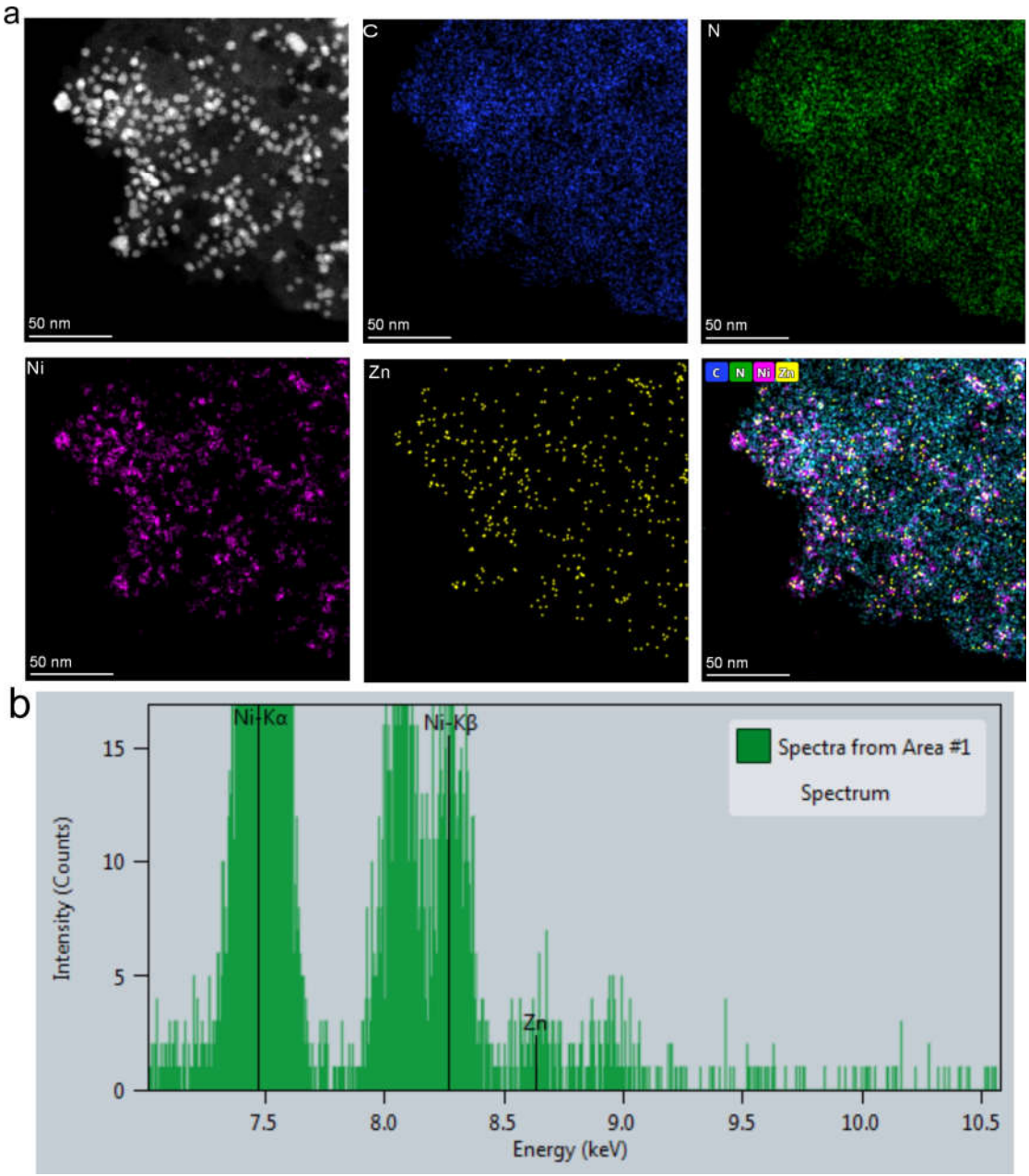

Figure S7. (a) TEM image and EDS mapping of Ni/Zn_1-NC in a wide region. (b) Corresponding EDX spectra of Ni/Zn_1-NC.

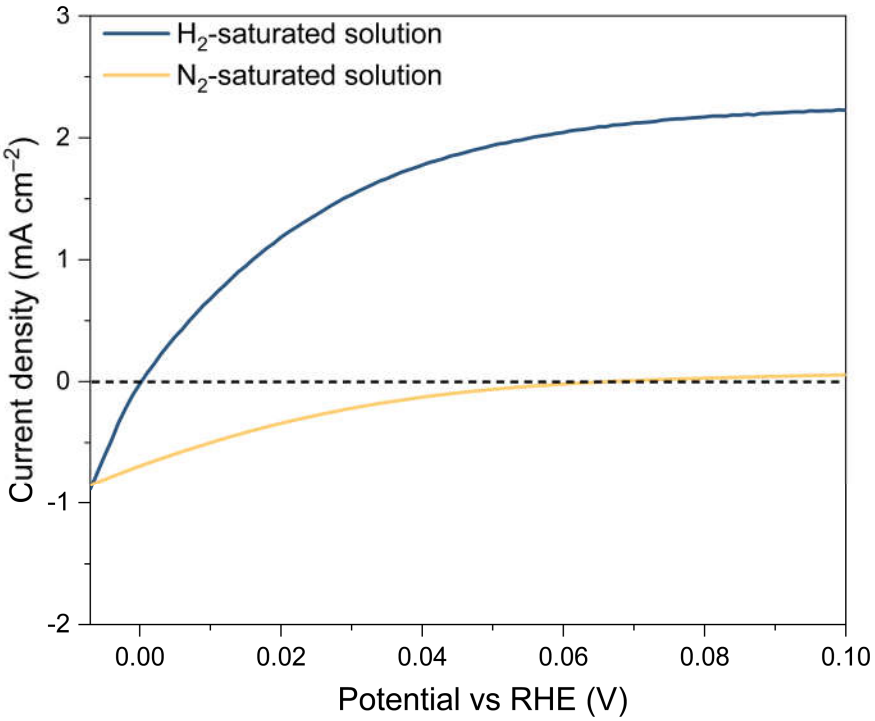

Figure S8. Polarization curves of Ni/Zn_1-NC in N_2-saturated 0.1 M KOH and in H_2-saturated 0.1 M KOH with a rotating speed of 1,600 rpm. The catalyst has a loading of 0.612 $mg_{catalyst}$ cm^{-2}.

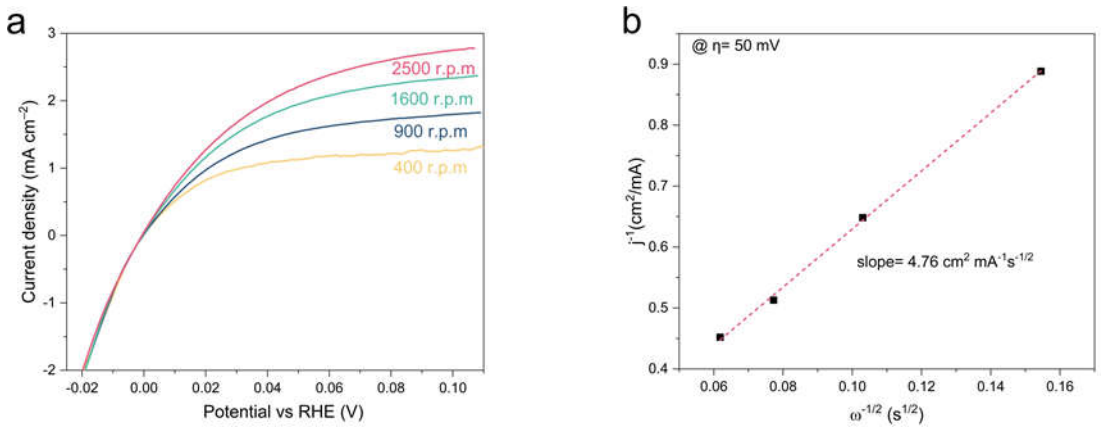

Figure S9. (a) HOR polarization curves of Ni/Zn_1-NC in 0.1 M H_2-saturated KOH with different rotation speeds. (b), Koutecky–Levich plot for Ni/Zn_1-NC at an overpotential of 50 mV.

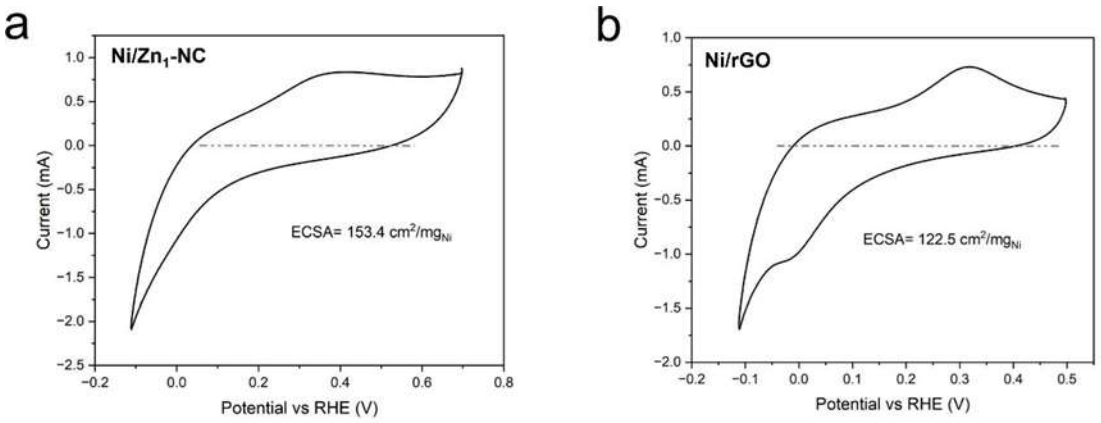

Figure S10. Cyclic voltammetry for the catalysts in 0.1 M N_2-saturated KOH with a scan rate of 50 mV s^{-1} with an overall catalyst loading of 0.612 $mg_{catalyst}$ cm^{-2}. The shaded area is used to estimate the electrochemical surface area (ECSA) since the difference between the backward and forward cathodic current corresponds to the transformation of α-$Ni(OH)_2$ to Ni and the charge density is reported to be 514 μC cm^{-2}. (a) the ECSA of Ni/Zn_1-NC; (b) the ECSA of Ni/rGO.

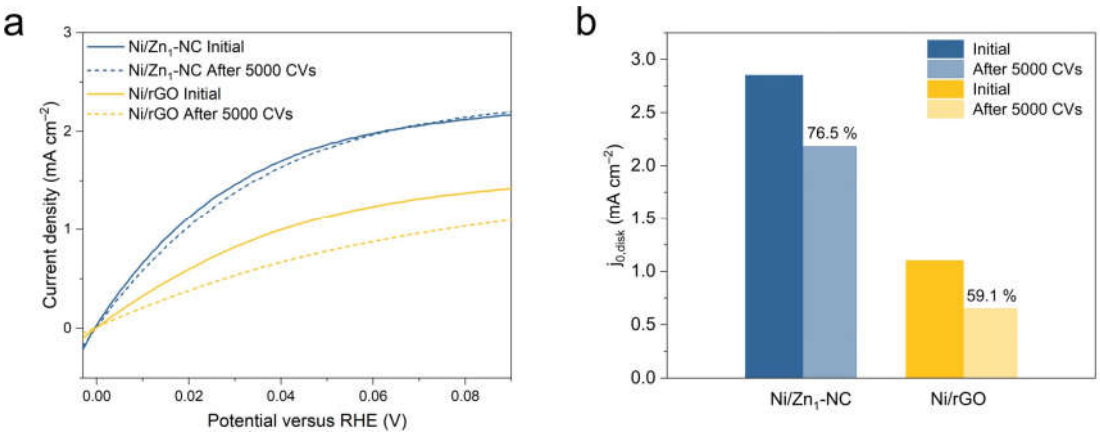

Figure S11. (a) ADT for the HOR in the presence of Ni/Zn_1-NC and Ni/rGO, during which 5,000 cyclic voltammetry (CV) scans were performed in the range of -1.0 V to -0.9 V relative to the silver-silver halide reference electrode (Ag/AgCl (V)), at a scanning rate of 50 mV s^{-1}. The solid curve represents the initial LSV, and the dashed curve represents the LSV after the durability test. (b) The bar plot shows a comparison of $j_{0,disk}$ before and after 5,000 CV scans in the presence of Ni/Zn_1-NC and Ni/rGO.

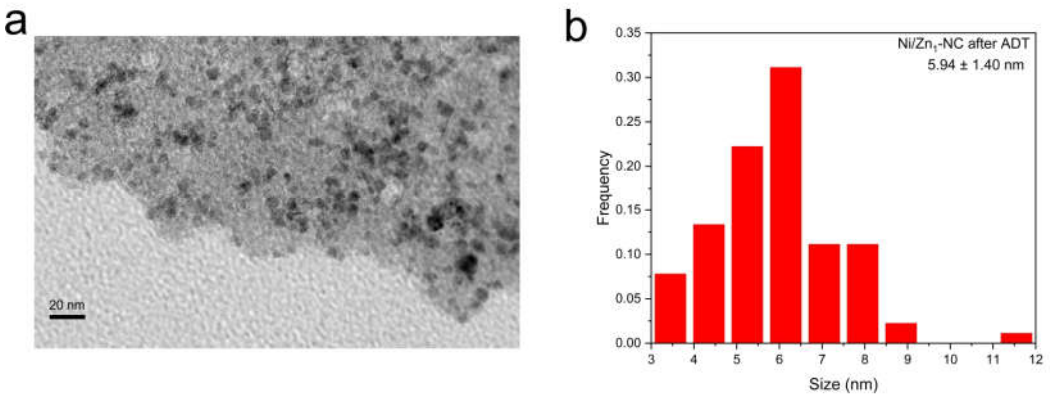

Figure S12. (a) TEM image of Ni/Zn_1-NC after ADT and (b) the size distribution of nanoparticles after ADT.

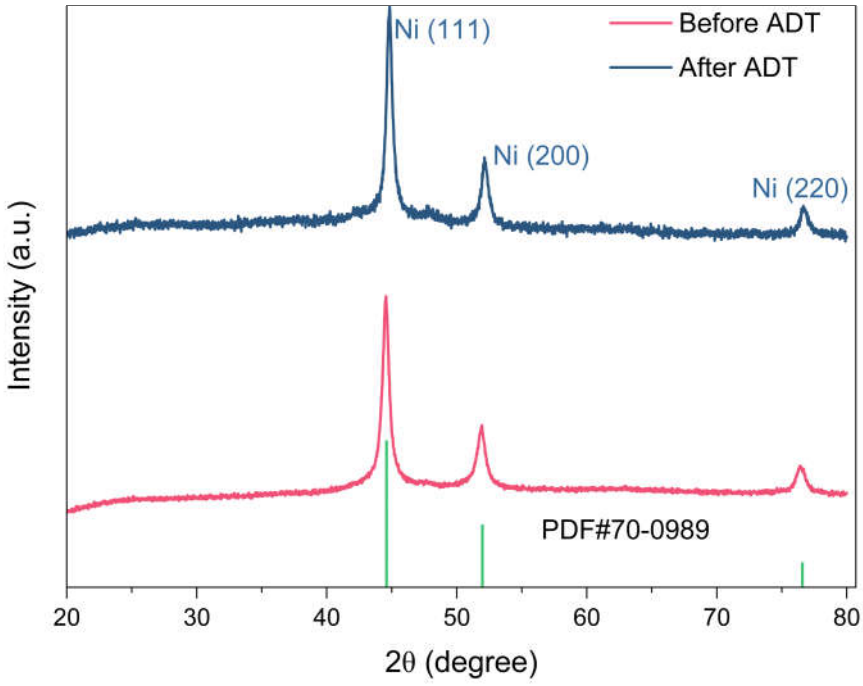

Figure S13. XRD pattern of Ni/Zn_1-NC before and after ADT.

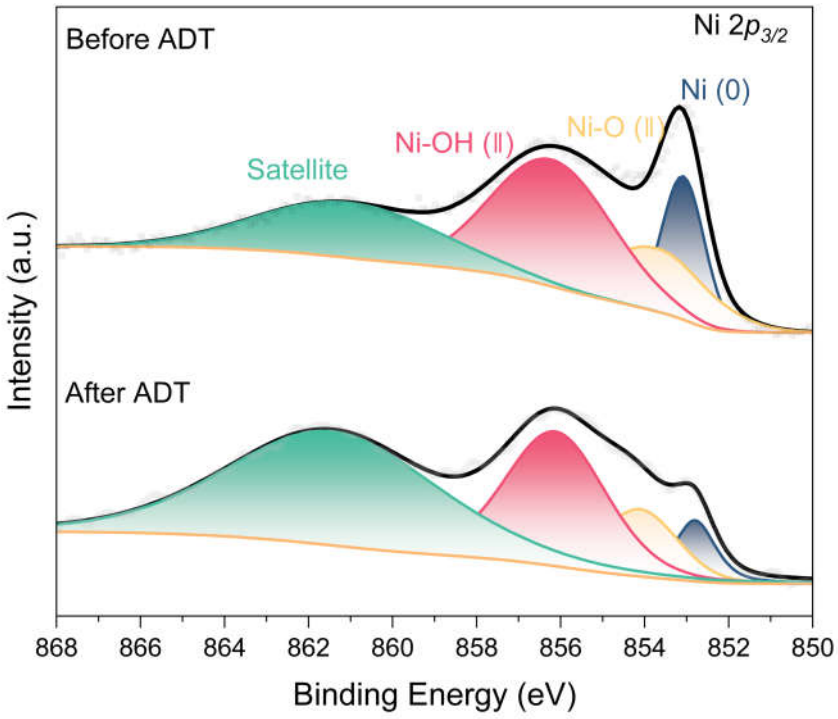

Figure S14. High resolution Ni $2p_{3/2}$ spectra of Ni/Zn_1-NC before and after ADT.

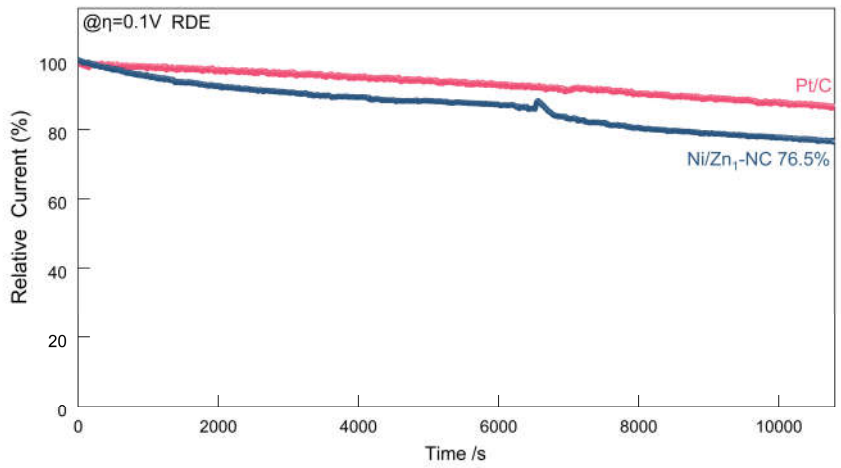

Figure S15. Relative chronoamperometry response of commercial Pt/C and Ni/Zn_1-NC in H_2-saturated 0.1 M KOH at 0.1 V versus RHE operated on the RDE.

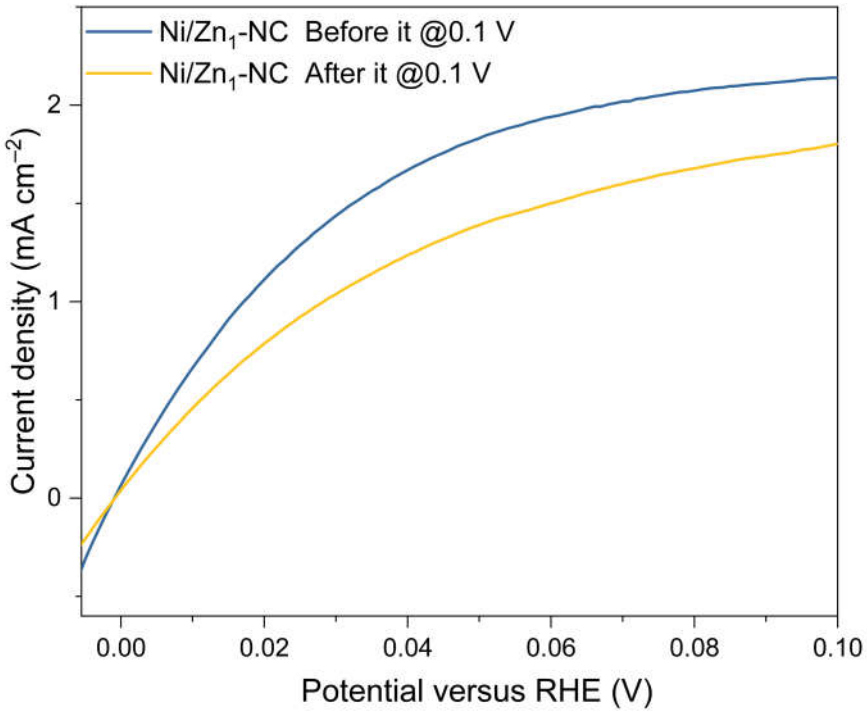

Figure S16. After durability test in H_2-saturated 0.1M KOH at 0.1 V versus RHE operated on RDE. The top line was the initial LSV, and the bottom line was the LSV after the durability test. The catalyst was Ni/Zn_1-NC.

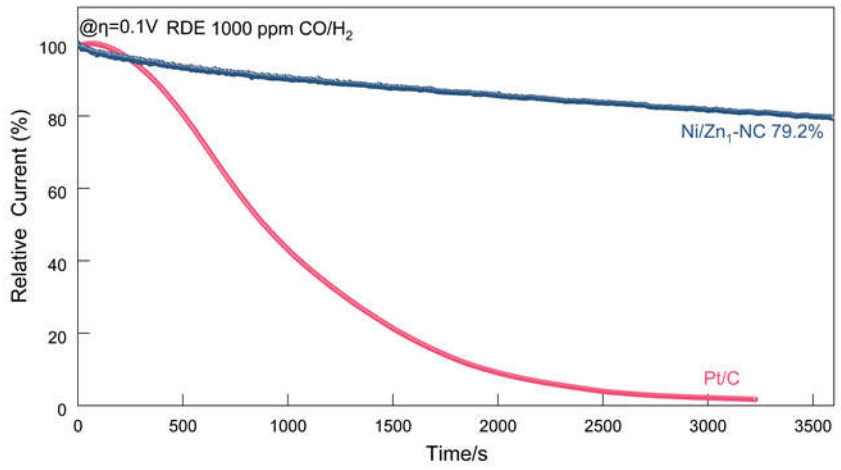

Figure S17. Relative chronoamperometry response of Pt/C and Ni/Zn_1-NC in 1000 ppm CO/H_2-saturated 0.1M KOH at 0.1 V versus RHE operated on RDE. The Pt/C catalyst loading was 20.4 $\mu g_{PGM}\ cm^{-2}$. The Ni/Zn_1-NC catalyst had a loading of 0.612 $mg_{catalyst}\ cm^{-2}$.

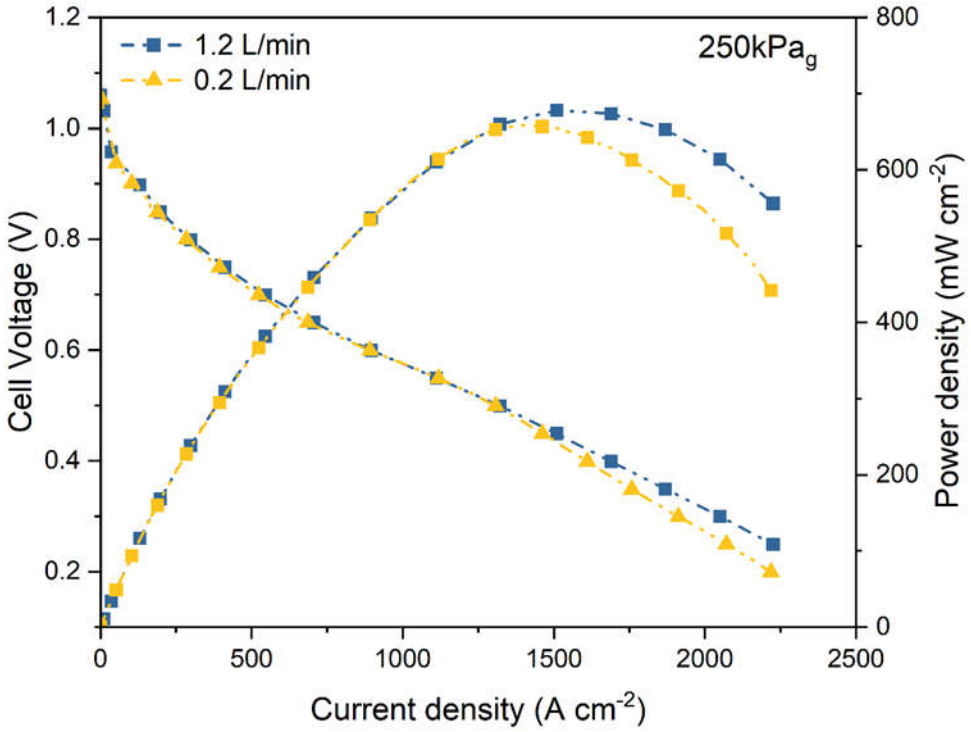

Figure S18. Fuel cell performance using Ni/Zn$_1$-NC as anode with Pt/C as cathode. Test condition: cell temperature at 95.0°C, cathode humidifier at 86.0°C, anode humidifier at 89.0°C. the flow rate is 0.2 L min^{-1} and 1.2 L min^{-1} on both sides, respectively. The back pressure was 250 kPa$_g$ on both sides.

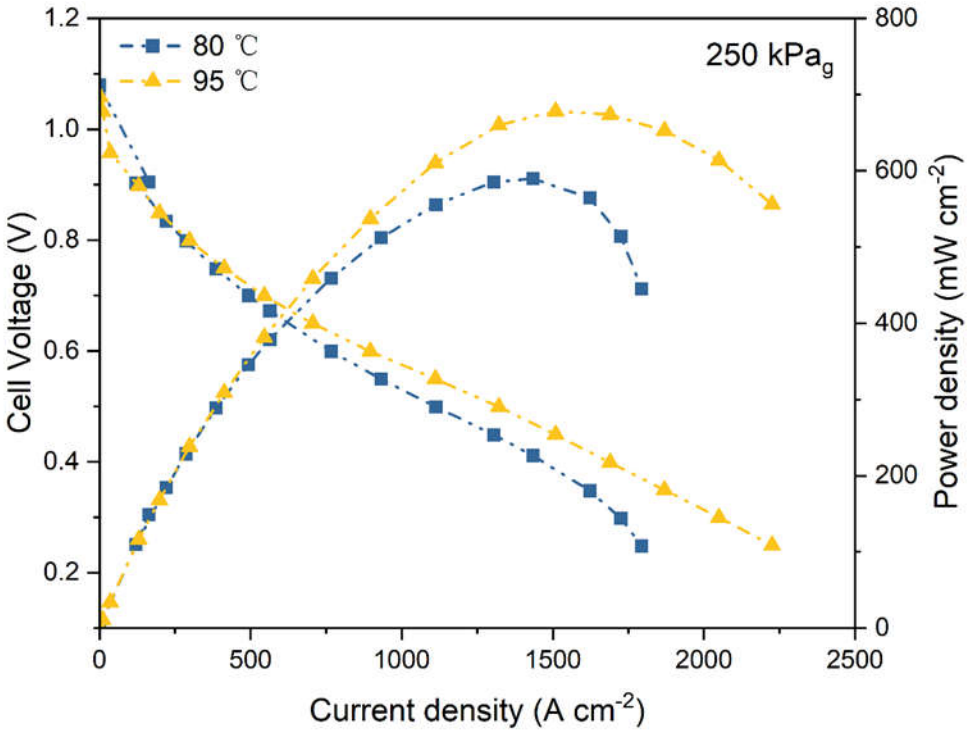

Figure S19. Fuel cell performance using Ni/Zn_1-NC as anode with Pt/C as cathode. The blue line test condition: cell temperature at 80.0°C, cathode humidifier at 76.0°C, anode humidifier at 74.0°C. The yellow line test condition: cell temperature at 95.0°C, cathode humidifier at 89.0°C, anode humidifier at 86.0°C. The flow rate is 1.2 L min^{-1} on both sides. The back pressure was 250 kPa_g on both sides.

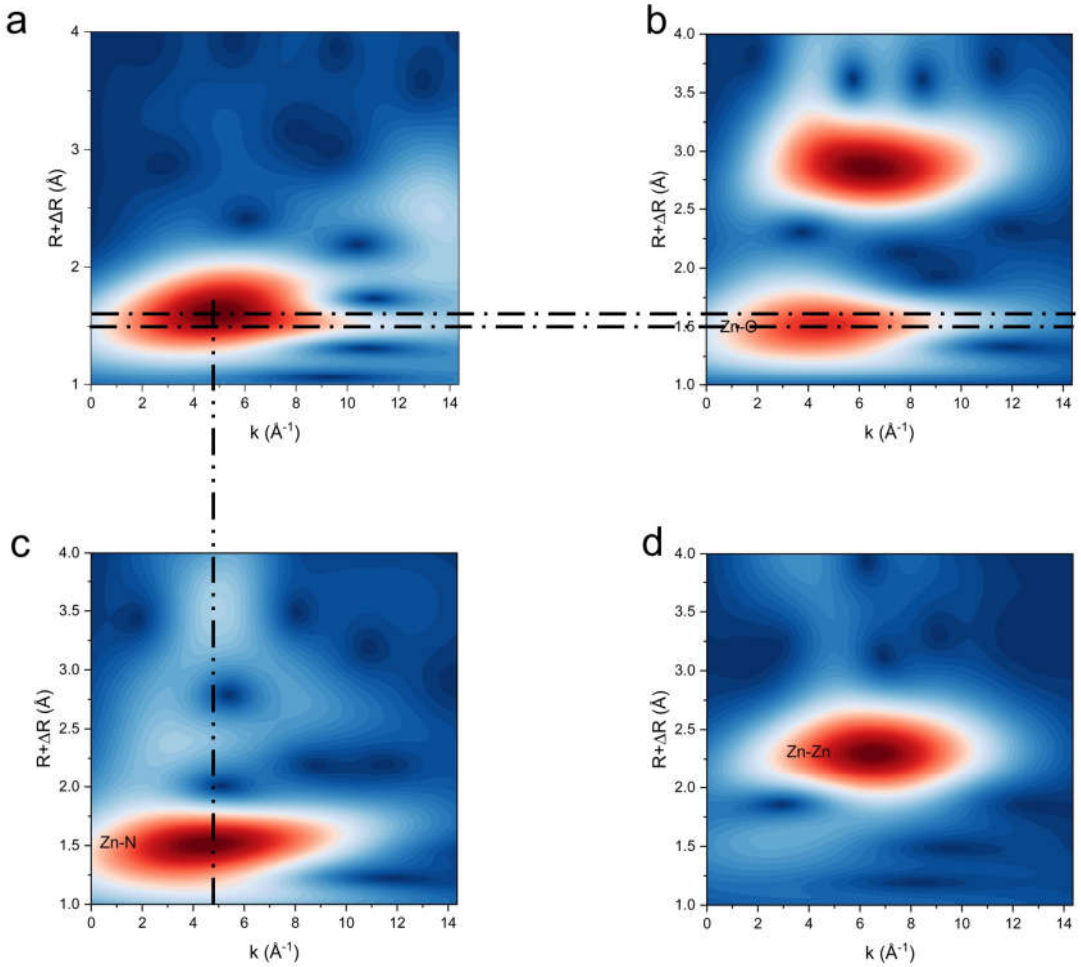

Figure S20. The wavelet transforms (WT) of K_3-weighted EXAFS spectra for (a)Zn_1-NC, (b) ZnO, (c) Zn Pc and (d) Zn foil.

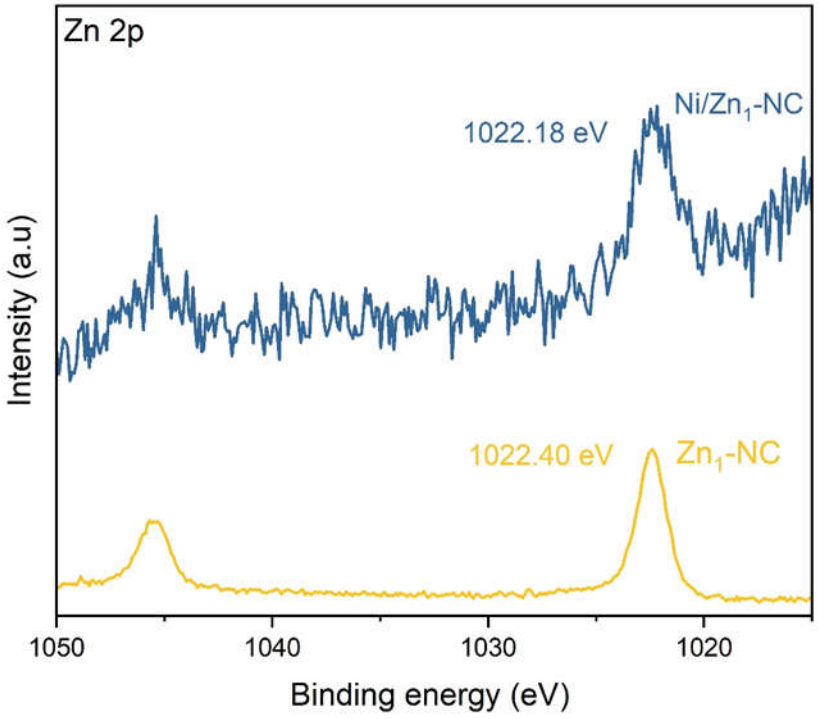

Figure S21. XPS spectra of Zn 2*p*. This data revealed that the underlying electron direction may be the transfer of electrons from Ni to Zn. This might be the result of the interaction between Ni and the carbon carrier.

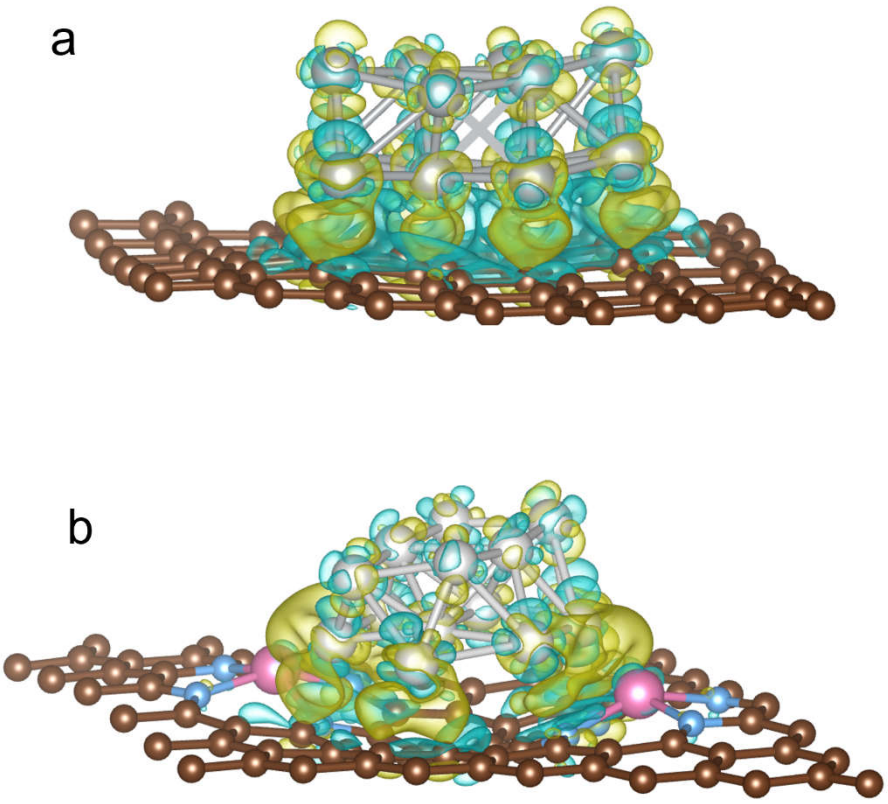

Figure S22. Difference of charge density in (a) Ni/Zn_1-NC and (b) Ni/rGO.

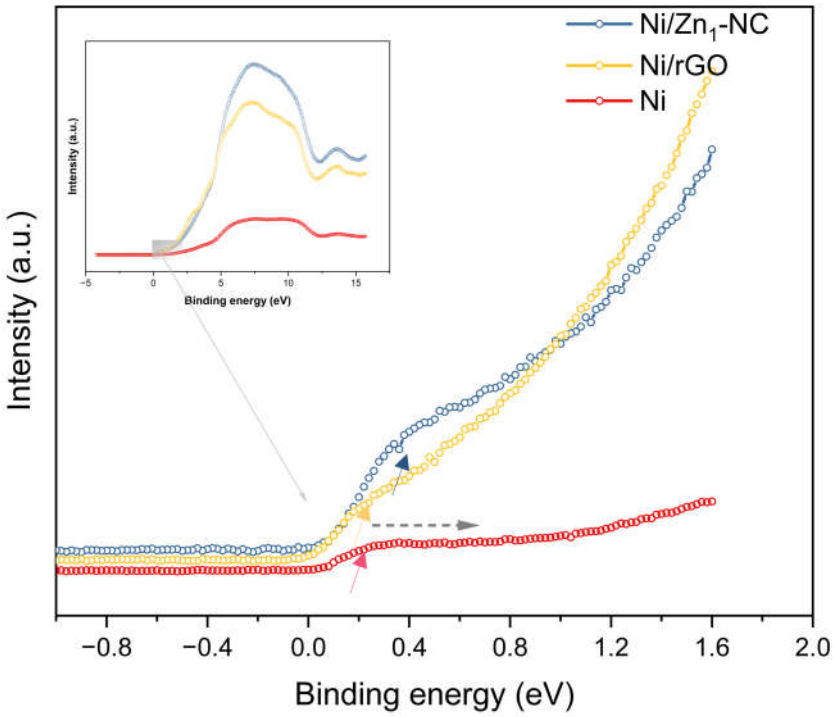

Figure S23.UPS results of Ni, Ni/rGO and Ni/Zn_1-NC.

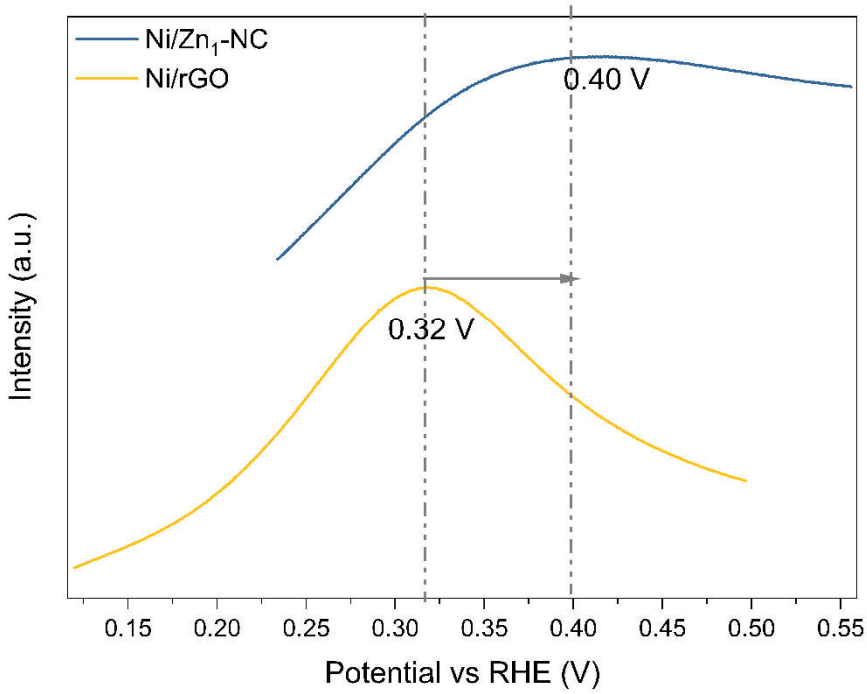

Figure S24. Anodic scans showing the oxidative adsorption of OH^- in N_2-saturated 0.1M KOH solution for Ni/Zn_1-NC and Ni/rGO.

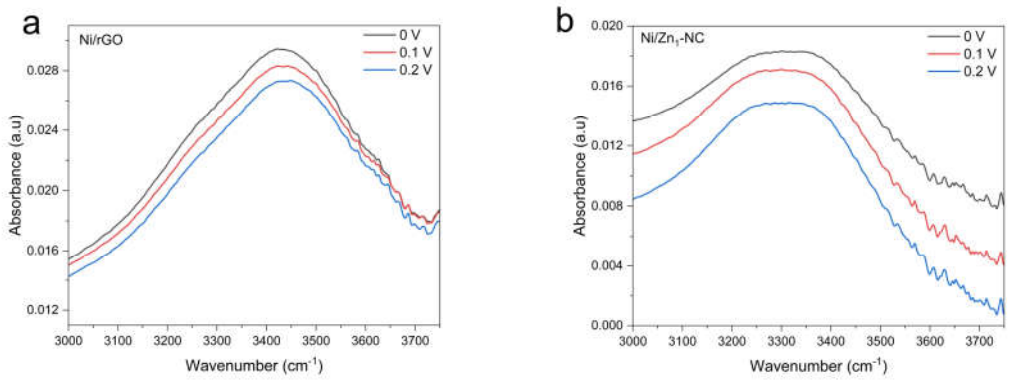

Figure S25. Raw data of *in-situ* ATR-SEIRAS. The background was determined at 0 V versus RHE. Then the potential was fixed at each potential (from 0 V to 0.2 V versus RHE) to acquire signals.

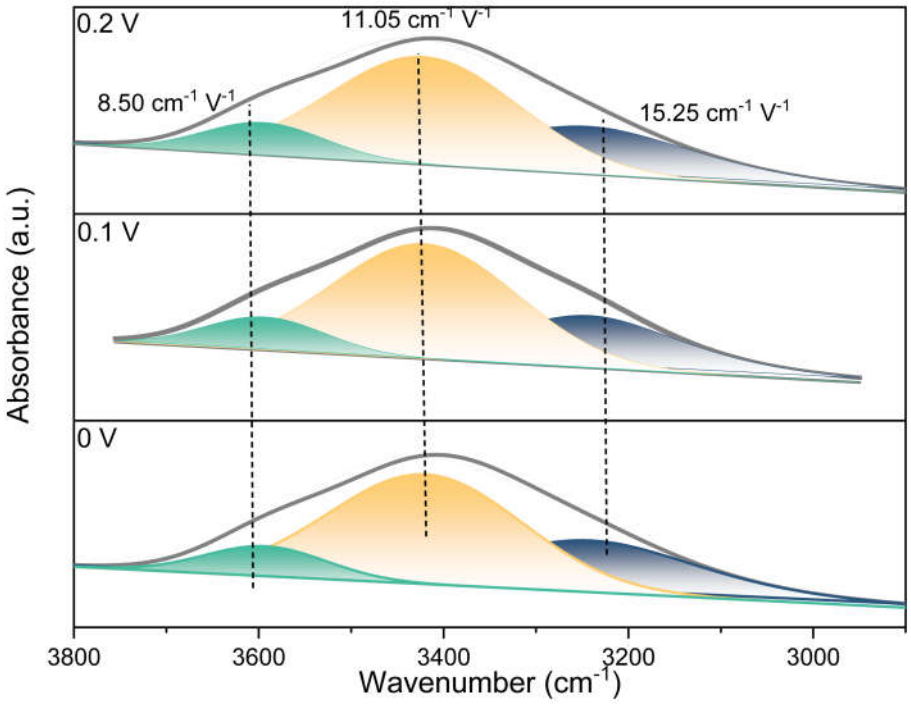

Figure S26. Fitting results of in situ SEIRAS for Ni/rGO. The Stark tuning rates are indicated.

Table S1. ICP-AES analysis results of metal loading of the Zn_1-NC.

Catalyst	Zn (wt.%)
Zn_1-NC	1.84

Table S2. EDS analysis results of relative element fraction of the Ni/Zn_1-NC.

Element	Ni Mass Fraction (%): Zn Mass Fraction (%)
Ni: Zn	22.54:0.54*

*The analysis of the absolute content was affected due to the presence of carbon in the carrier web carrying the sample.

Table S3. Analysis results of weight ratio of Ni/Zn_1-NC and Ni/rGO.

Catalyst	Text 1 Ni (%)	Text 2 Ni (%)	Text 3 Ni (%)	average Ni (%)
Ni/Zn_1-NC	50.1	48.5	/	49.3
Ni/rGO	50.7	51.3	50.5	50.8

Table S4. The mass activities at 50 mV and $j_{0,s}$ for Catalysts.

Catalysts	j_k (mA cm^{-2})	j_0 (mA cm^{-2})	$j_{0,s}$ (μA cm^{-2})	$j_{k,m}$ (mA mg^{-1})	**transfer coefficient (α)**
Ni/rGO	6.1	1.0	26.6	19.7	0.99
Ni/Zn_1-NC	16.9	3.13	68.0	56.1	0.93

Table S5. ICP-AES analysis results of metal loading of the AEMFC.

Catalyst	Text 1 (mg/cm^2)	Text 2 (mg/cm^2)	Text 3 (mg/cm^2)	Average (mg/cm^2)
Pt	0.2313	0.1987	0.2207	0.22
Ni	1.3318	1.3237	1.3297	1.33

Table S6. Comparison of the H_2-O_2 AEMFCs performances between Ni/Zn_1-NC and the reported Ni-based anode.

Anode catalyst Loading Catalyst/Ni mg cm^{-2}	Cathode Catalyst	Cell Temp °C	Backpressure Anode/Cathode, kPa_g	PPD mW cm^{-2}	Reference
Ni/Zn_1-NC/1.33	**Pt/C**	**95/80**	**250/250**	**678/590**	**This wok**
Ni-H_2-NH_3/6.40	Pt/C	95	250/250	628	[10]
NiCuCr/C/9.00	Pt/C	80	200/200	577	[11]
Co-$MoNi_4$/6.00	Pt/C	95	200/200	525	[12]
Ni@CNx/15.00	Pt/C	80	200/200	480	[13]
Cr-$MoNi_4$/6.00	Pt/C	90	200/200	477	[14]
Ni_3N/4.00	Pt/C	90	200/200	532	[15]
$Ni_{52}Mo_{13}Nb_{35}$/4.00	Pt/C	90	200/200	390	[16]
Ni@Oi-Ni/1.30	Pt/C	80	200/200	274	[17]
Mo-decorated Ni_3N/	Pt/C	70	100/100	180	[18]
Ni@NC/PEIXC/1.10	Pt/C	80	200/200	241	[19]
Ni@C-500 °C/5.0	Pt/C	80	200/200	160	[20]
Ni_4Mo/TiO_2/1.35	Pt/C	80	200/200	520	[21]
NiCu/KB/4.00	Pd/C	80	138/138	350	[22]
NiMo/KB/4.00	Pd/C	70	138/138	120	[23]

Table S7. Comparison of our cell with other state-of-the-art AEMFCs

Anode Catalysts	Anode Loading (mg_{PGM} cm^{-2})	PGM Utilization[a] (W mg_{PGM}^{-1})	Reference
Ni/Zn_1-NC	/	**3.08**	**This Work**
Pt-RuO_2	0.123	1.07	Nanoscale Horiz. **5**, 316-324 (2020).
PtRu/N-C	0.2	1.39	Adv. Mater. Inter. **7**, 2000310 (2020).
Pt_5Ru_5-300/C	0.152	3.15	J. Am. Chem. Soc. **145**, 27500–27511 (2023).
PtRu/C	0.2	2.63	Nat. Commun. **11**, 5651 (2020).
Ru_7Ni_3/C	0.2	3.383	Nat. Commun. **11**, 5651 (2020).
Ru/meso C	0.1	1.854	J. Power Sources. **461**, 228147 (2020).
CeO_x-Pd/C	0.38	1.082	Adv. Funct. Mater. **30**, 2002087 (2020).
RhMo NSs	0.2	3.8	Nat Commun. **14**, 1761 (2023).
$Pd_{0.33}Ir_{0.67}$/C	0.2	1.028	J. Mater. Chem. A**7**, 3161-3169 (2019).
IrNi@PdIr/C	0.1	0.778	Nanoscale.**10**, 4872-4881 (2018).
RuNi/NC	1	0.45	Sci. Adv. **8**, eabm3779 (2022).
PtRu/C	0.6	1.85	Chem. Commun. **53**, 11771-11773 (2017).
PtRu/C	0.4	3	ACS Energy Letters. **4**, 1251-1257 (2019).
Pt/C	0.4	2.75	Nat. Commun. 10, 1506 (2019).
Pd/CeO_2+C	0.5	0. 618	Energies. **13**, 582 (2020).
PtRu/C	0.4	1	ACS Catal. **7**, 6485-6492 (2017).
Ni@C	/	0.4	ACS Appl. Mater. Interfaces. **12**, 31575-31581 (2020).
NiMo/KB	/	0.6	J. Mater. Chem. A **5**, 24433-24443 (2017).
NiCu/KB	/	1.75	Sustain. Energy Fuels. **2**, 2268-2275 (2018).

a: calculated by dividing peak power density by the sum of PGM loading in both electrodes.

Table S8. Comparison of the H_2-Air AEMFCs performances between Ni/Zn_1-NC and the reported Ni-based anode.

Anode catalyst Loading Catalyst/Ni mg cm^{-2}	Cathode Catalyst	Cell Temp ℃	Backpressure Anode/Cathode, kPa_g	PPD mW cm^{-2}	Reference
Ni/Zn_1-NC/1.33	**Pt/C**	**95/80**	**250/250**	**510/406**	**This wok**
Ni-H_2-NH_3/6.40	Pt/C	95	250/250	500	[10]
NiCuCr/C/9.00	Pt/C	80	200/200	146	[11]
Co-$MoNi_4$/6.00	Pt/C	95	200/200	390	[12]
Ni@CNx/15.00	Pt/C	80	200/200	/	[13]
Cr-$MoNi_4$/6.00	Pt/C	90	200/200	/	[14]
Ni_3N/4.00	Pt/C	90	200/200	/	[15]
$Ni_{52}Mo_{13}Nb_{35}$/4.00	Pt/C	90	200/200	253	[16]
Ni@Oi-Ni/1.30	Pt/C	80	200/200	/	[17]
Mo-decorated Ni_3N/	Pt/C	70	100/100	/	[18]
Ni@NC/PEIXC/1.10	Pt/C	80	200/200	/	[19]
Ni@C-500 °C/5.0	Pt/C	80	200/200	/	[20]
Ni_4Mo/TiO_2/1.35	Pt/C	80	200/200	/	[21]
NiCu/KB/4.00	Pd/C	80	138/138	/	[22]
NiMo/KB/4.00	Pd/C	70	138/138	/	[23]

Table S9. Comparison of the stability between Ni/Zn_1-NC and reported Ni-based anode.

Anode catalyst Loading Catalyst/Ni mg cm^{-2}	Cathode Catalyst	Cell Temp °C	Backpressure Anode/Cathode, kPa_g	Stability	Reference
Ni/Zn_1-NC/1.33	**Pt/C**	**80**	**250/250**	**100 h@200 mA cm^{-2}**	**This wok**
Ni-H_2-NH_3/6.40	Pt/C	95	250/250	40 h@0.7 V	[10]
NiCuCr/C/9.00	Pt/C	80	200/200	156 h@0.7 V	[11]
Co-$MoNi_4$/6.00	Pt/C	95	200/200	/	[12]
Ni@CNx/15.00	Pt/C	80	200/200	100 h@200 mA cm^{-2}	[13]
Cr-$MoNi_4$/6.00	Pt/C	90	200/200	/	[14]
Ni_3N/4.00	Pt/C	90	200/200	25 h@100 mA cm^{-2}	[15]
$Ni_{52}Mo_{13}Nb_{35}$/4.00	Pt/C	90	200/200	50 h@200 mA cm^{-2}	[16]
Ni@Oi-Ni/1.30	Pt/C	80	200/200	/	[17]
Mo-decorated Ni_3N/	Pt/C	70	100/100	30 h@0.7 V	[18]
Ni@NC/PEIXC/1.10	Pt/C	80	200/200	/	[19]
Ni@C-500 °C/5.0	Pt/C	80	200/200	120 h@0.7 V	[20]
Ni_4Mo/TiO_2/1.35	Pt/C	80	200/200	100 h@400 mA cm^{-2}	[21]
NiCu/KB/4.00	Pd/C	80	138/138	115 h@0.7 V	[22]
NiMo/KB/4.00	Pd/C	70	138/138	/	[23]

Reference

1. Wang W, et al. Intrinsic Carbon-Defect-Driven Electrocatalytic Reduction of Carbon Dioxide. *Adv Mater* **31**,19 (2019).

2. Ni, W. et al. Efficient Hydrogen Oxidation Catalyzed by Strain-Engineered Nickel Nanoparticles. *Angew Chem Int Ed* **59**, 10797-10801 (2020).

3. John C, et al. High-performance Ionomerless Cathode Anion-exchange Membrane Fuel Cells with Ultra-low-loading Ag–Pd Alloy Electrocatalysts. *Nature Energy* **8**, 1262–1272 (2023).

4. Wan, T. H.; Saccoccio, M.; Chen, C.; Ciucci, F., Influence of the Discretization Methods on the Distribution of Relaxation Times Deconvolution: Implementing Radial Basis Functions with DRTtools. Electrochimica Acta 2015, 184, 483-499.

5. Saccoccio, M.; Wan, T. H.; Chen, C.; Ciucci, F., Optimal Regularization in Distribution of Relaxation Times applied to Electrochemical Impedance Spectroscopy: Ridge and Lasso Regression Methods - A Theoretical and Experimental Study. Electrochimica Acta 2014, 147, 470-482.

6. Kresse G, et al. Efficient Iterative Schemes for Ab Initio Total-Energy Calculations using a Plane-Wave Basis Set. *Phys Rev B* **54**, 11169-11186 (1996).

7. Kresse G, et al. Ab Initio Molecular Dynamics for Liquid Metals. *Phys Rev B* **49**, 14251-14269 (1994).

8. Perdew J.P, et al. Generalized Gradient Approximation Made Simple. *Phys Rev Lett* **77**, 3865-3868 (1996).

9. Hammer, B, et al. Improved Adsorption Energetics within Density Functional Theory using Revised Perdew-Burke-Ernzerhof Functionals. *Phys Rev B* **59**, 7413-7421 (1999).

10. Ni W, et al. An Efficient Nickel Hydrogen Oxidation Catalyst for Hydroxide Exchange Membrane Fuel Cells. *Nat Mater* **21**, 804-810 (2022).

11. Wang X-D, et al. Tuning the Apparent Hydrogen Binding Energy to Achieve High Performance Ni-based Hydrogen Oxidation Reaction Catalyst. *Nature Communications* **15**, 1137 (2024).

12. Yang Y, et al. Suppressing Electron Back-donation for a Highly CO-tolerant Fuel Cell Anode Catalyst via Cobalt Modulation. *Angew Chem Int Ed* **61**, e202208040 (2022).

13. Gao Y, et al. A Completely Precious Metal-free Alkaline Fuel Cell with Enhanced Performance Using a Carbon-coated Nickel Anode. *Proc Natl Acad Sci USA* **119**, e2119883119 (2022).

14. Wang Y-H, et al. Efficient NH_3-Tolerant Nickel-Based Hydrogen Oxidation Catalyst for Anion Exchange Membrane Fuel Cells. *J. Am. Chem. Soc* **145**, 17485–17494 (2023).

15. Zhang X-L, Hu S-J, Wang Y-H, Shi L, Yang Y, Gao M-R. Plasma-Assisted Synthesis of Metal Nitrides for an Efficient Platinum-Group-Metal-Free Anion-Exchange-Membrane Fuel Cell. *Nano Lett* **23**, 107- 115 (2023).

16. Gao F-Y, et al. Nickel–Molybdenum–Niobium Metallic Glass for Efficient Hydrogen

Oxidation in Hydroxide Exchange Membrane Fuel Cells. *Nat Catal* **5**, 993-1005 (2022).
17. Men Y, et al. Oxygen-Inserted Top-Surface Layers of Ni for Boosting Alkaline Hydrogen Oxidation Electrocatalysis. *J Am Chem Soc* **144**, 12661-12672 (2022).
18. Chen F, et al. Mo-Decorated Ni_3N Nanostructures for Alkaline Polymer Electrolyte Fuel Cells. *ACS Appl Nano Mater* **4**, 11473-11479 (2021).
19. Wang J, et al. Ultrafine Nickel Nanoparticles Encapsulated in N-Doped Carbon Promoting Hydrogen Oxidation Reaction in Alkaline Media. *ACS Catal* **11**, 7422-7428 (2021).
20. Gao Y-F, et al. Improving the Antioxidation Capability of the Ni Catalyst by Carbon Shell Coating for Alkaline Hydrogen Oxidation Reaction. *ACS Appl Mater Interfaces* **12**, 31575-31581 (2020).
21. Tian X-Y, et al. Metal-support Interaction Boosts the Stability of Ni-based Electrocatalysts for Alkaline Hydrogen Oxidation. *Nature Communications* **15**, 76 (2024).
22. Roy A, et al. Nickel–copper Supported on a Carbon Black Hydrogen Oxidation Catalyst Integrated into an Anion-exchange Membrane Fuel Cell. *Sustain Energy Fuels* **2**, 2268-2275 (2018).
23. Kabir S, et al. Platinum Group Metal-free NiMo Hydrogen Oxidation Catalysts: High Performance and Durability in Alkaline Exchange Membrane Fuel Cells. *J Mater Chem A* **5**, 24433-24443 (2017).